Spectrochimica Acta Part A: Molecular and Biomolecular Spectroscopy 286 (2023) 122002

Contents lists available at ScienceDirect

Spectrochimica Acta Part A: Molecular and Biomolecular Spectroscopy

journal homepage: www.journals.elsevier.com/spectrochimica-acta-part-a-molecular-and-biomolecular-spectroscopy

Fast calculation of spectral optical properties and pigment content detection in human normal and pathological kidney

Ana R. Botelho [a], Hugo F. Silva [b], Inês S. Martins [c], Isa C. Carneiro [d,e], Sónia D. Carvalho [d,f], Rui M. Henrique [d,g], Valery V. Tuchin [h,i,j], Luís M. Oliveira [a,k,*]

[a] Physics Department, Polytechnic of Porto – School of Engineering (ISEP), Porto, Portugal
[b] Porto University, School of Engineering, Porto, Portugal
[c] Center for Innovation in Engineering and Industrial Technology, ISEP, Porto, Portugal
[d] Department of Pathology and Cancer Biology and Epigenetics Group, Portuguese Oncology Institute of Porto, Porto, Portugal
[e] Department of Pathological, Cytological and Thanatological Anatomy, Polytechnic of Porto – School of Health (ESS), Porto, Portugal
[f] Department of Pathology, Santa Luzia Hospital (ULSAM), Viana do Castelo, Portugal
[g] Department of Pathology and Molecular Immunology, Porto University – Institute of Biomedical Sciences Abel Salazar, Porto, Portugal
[h] Science Medical Center, Saratov State University, Saratov, Russian Federation
[i] Laboratory of Laser Molecular Imaging and Machine Learning, Tomsk State University, Tomsk, Russian Federation
[j] Laboratory of Laser Diagnostics of Technical and Living Systems, Institute of Precision Mechanics and Control, FRC "Saratov Research Centre of Russian Academy of Sciences," Saratov, Russian Federation
[k] Institute for Systems and Computer Engineering, Technology and Science (INESC TEC), Porto, Portugal

HIGHLIGHTS

- Simple and fast calculation of the broadband spectral optical properties of biological tissues can be made using experimental spectra acquired from ex vivo samples.
- The spectral optical properties provide valuable information to develop light propagation models to be used in diagnostic and treatment procedures.
- The spectral absorption coefficient contains information about the tissue components, namely hemoglobin (blood), DNA, lipids, water and melanin-like pigments.
- Differentiated hemoglobin (blood) and melanin-like pigment contents can be retrieved from the analysis of the spectral absorption coefficient of normal and pathological tissues.
- Estimation of differentiated absorption coefficient spectra for normal and pathological tissues can be made using noninvasive reflectance spectra in deep-learning algorithms to obtain a diagnosis *in vivo*.

GRAPHICAL ABSTRACT

Variation of melanin and lipofuscin contents between healthy and pathological kidney

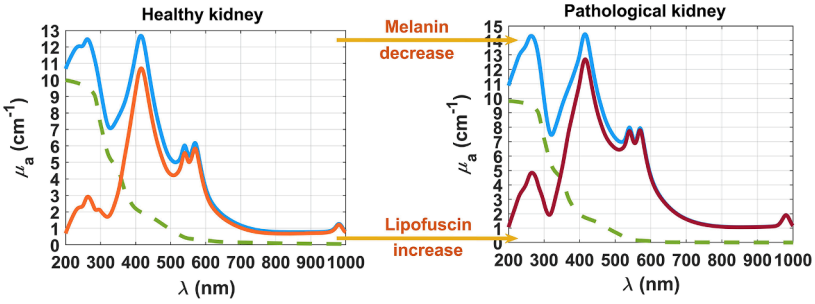

* Corresponding author at: Physics Department, Polytechnic of Porto – School of Engineering (ISEP), Porto, Portugal.
E-mail address: lmo@isep.ipp.pt (L.M. Oliveira).

https://doi.org/10.1016/j.saa.2022.122002
Received 29 May 2022; Received in revised form 11 October 2022; Accepted 13 October 2022
Available online 18 October 2022

ARTICLE INFO

Keywords:
Human kidney
Chromophobe renal cell carcinoma
Spectral absorption coefficient
Melanin
Lipofuscin
Renal cancer discrimination

ABSTRACT

A fast calculation method was used to obtain the spectral optical properties of human normal and pathological (chromophobe renal cell carcinoma) kidney tissues. Using total transmittance, total reflectance and collimated transmittance spectra acquired from *ex vivo* kidney samples, the spectral optical properties of both tissues, namely the absorption, the scattering and the reduced scattering coefficients, as well as the scattering anisotropy, dispersion and light penetration depth, were calculated between 200 and 1000 nm. Analysis of the mean absorption coefficient spectra of the kidney tissues showed that both contain melanin and lipofuscin, and that 83 % of the melanin in the normal kidney converts into lipofuscin in the pathological kidney.

1. Introduction

The kidney is an organ of vital importance in the human body, since it is responsible for the regulation, filtering and excretion of toxic substances, excess of medical drugs and certain biological and metabolic products that flow in the blood stream. There are a significant number of pathologies associated with the kidney. In the case of renal cancers, renal cell carcinoma which by itself has some variants such as cromophobe renal cell carcinoma (CRCC), is one of the most common to occur [1]. Renal cell carcinoma is ranked in the 13th place in the list of most common cancers worldwide, having an annual incidence of about 330,000 people worldwide [2], and being responsible for more than 100,000 deaths [3]. To reduce these numbers, it is necessary to perform periodic screening exams, so that the renal cell carcinoma and other types of kidney cancers can be detected in their early stages of development, and adequate treatments can be applied with high effectiveness as soon as possible to increase the life expectancy of the patient. Fig. 1 presents two histological photographs taken at the Portuguese Oncology Institute of Porto (Portugal) with 15x and 20x magnification at the microscope from kidney tissues, where the healthy kidney (Fig. 1 A) and the kidney with a CRCC (Fig. 1 B) are seen.

A new line of fast and effective diagnostic methods, based on optical technologies, such as 3-dimensional imaging or broadband spectroscopy, can be developed to be used in periodic screening exams for renal cancer detection. The benefits of developing such methods are the low cost and compact instrumentation that can be reused, high reliability in the established diagnose, and the use of noninvasive or minimally invasive procedures. Regarding the spectroscopy approach, it is first necessary to quantify the spectral optical properties both for the normal and for the diseased kidney and compare them to find out differences, which can be used in a diagnostic procedure. The estimation of the spectral optical properties, both for the healthy and for the CRCC kidney, can be made *in vivo* through the use of machine learning (ML) algorithms that perform such estimation based only on minimally invasive diffuse reflectance measurements [4,5]. The *in vivo* diffuse reflectance spectra of the kidney to be used in the ML algorithms can be acquired in a minimally invasive procedure, by making a small incision on the abdominal wall cavity and in the tissues that are located above the kidney, so that the optical sensor can be introduced and placed in contact with this organ. During the learning process of those ML algorithms, reference optical properties of the tissues need to be available for comparison to increase the estimation accuracy [5]. Such reference optical properties need to be obtained through another process, such as from spectral measurements acquired from *ex vivo* samples. Considering this procedure of estimating the optical properties from *ex vivo* spectral measurements there are different methods available. Within these methods, the most traditional are the inverse simulations, which use certain algorithms, such as the Monte Carlo [6] or the Adding-Doubling [7]. Although these algorithms are much popular and accurate, they are time and computer consuming, since the estimations are made for a single wavelength at a time. A faster method, which is based on the diffusion approximation, allows the calculation of the entire spectra of most of the optical properties at once [8–10].

With the objective of evaluating the spectral optical properties of the healthy and the CRCC kidney tissues and determine characteristic differences between the two tissues, this last method was used in the present study, as described in section 2.

2. Materials and methods

2.1. Sample collection and preparation

The tissue samples used in the present study were collected from surgical kidney resections of 10 adult patients under treatment at the Portuguese Oncology Institute of Porto (Portugal). Those patients have previously signed a written consent to use the collected tissues in research and diagnostic procedures. The study has been approved by the Ethics Committee of that institution.

Using a cryostat (model CM1850 UV from Leica™, Wetzlar, Germany), 10 healthy and 10 pathological samples were prepared from the

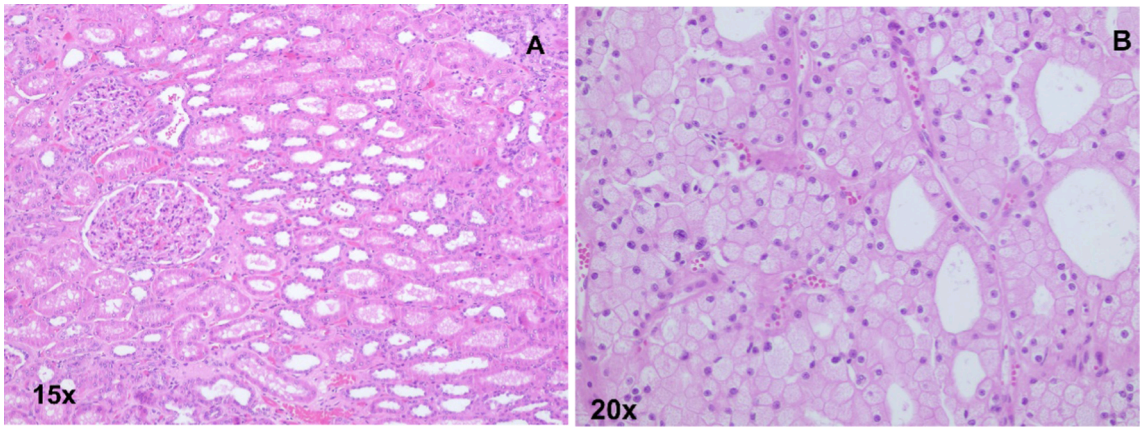

Fig. 1. Histological photographs of the human kidney, showing the healthy kidney with characteristic corpuscle (spherical structures that filter blood) and tubules (A) and CRCC showing confluent solid growth composed of pale cells with sharply defined plant-like cell borders (B).

surgical resections. These samples had approximated circular form ($\Phi \approx$ 1 cm), and a uniform thickness ($d = 0.5$ mm) and were placed in saline before measurements to keep their natural hydration.

2.2. Spectral measurements

To perform the necessary spectral measurements for the calculation of the optical properties of the kidney tissues, three experimental setups were used. Those setups are configured to measure the total transmittance (T_t), the total reflectance (R_t) and the collimated transmittance (T_c) spectra of the tissue samples, and were previously described by *Martins et al.* [10]. Each of the 20 tissue samples, 10 from the healthy kidney and 10 from the CRCC kidney, was submitted to spectral measurements between 200 and 1000 nm with each of the three experimental setups. Considering the three spectra obtained with each setup from a particular sample, calculations were made to obtain the corresponding spectral optical properties. Such calculations are described in section 3.

3. Theory/calculation

With the objective of obtaining statistical results for the spectral optical properties of both kidney tissues, and since 10 spectra were acquired with each setup both from the healthy and from the pathological kidney, the calculations described in this section were performed for each tissue sample and then averaged at the end.

Considering a particular tissue sample and the T_t, R_t and T_c spectra that were acquired from it, the optical properties for each sample were obtained through the following sequence of calculations.

a) The absorption coefficient spectrum ($\mu_a(\lambda)$) was calculated with the following relation [10]:

$$\mu_a(\lambda) = \frac{[1 - (T_t(\lambda) + R_t(\lambda))]}{d} \tag{1}$$

where d represents the sample thickness (0.05 cm).

b) The scattering coefficient spectrum ($\mu_s(\lambda)$) was obtained from the T_c spectrum through the Bouguer-Beer-Lambert (BBL) law [10–14], as follows:

$$\mu_s(\lambda) = -\frac{ln(T_c(\lambda))}{d} - \mu_a(\lambda) \tag{2}$$

c) There is no direct relation to calculate the reduced scattering coefficient ($\mu'_s(\lambda)$) from experimental measurements, but since its wavelength dependence is well described by a combination of the Rayleigh and Mie scattering regimes as accounted in the following relation [15], it can be estimated through inverse Adding-Doubling simulations at discrete wavelengths within the spectral range of interest and then fitted by such a curve [8–10]:

$$\mu'_s(\lambda) \equiv (1 - g(\lambda)) \times \mu_s(\lambda) = a \times \left(f_{Ray} \times \left(\frac{\lambda}{500nm} \right)^{-4} + (1 - f_{Ray}) \times \left(\frac{\lambda}{500nm} \right)^{-b_{Mie}} \right) \tag{3}$$

where $g(\lambda)$ is the spectral scattering anisotropy factor, $a = \mu'_s$ (λ = 500 nm), f_{Ray} is the Rayleigh scattering fraction and b_{Mie} is the exponent related to the mean size of the Mie scatterers. Considering the spectral range between 200 and 1000 nm, simulations were made at each 50 nm in the present study to obtain the discrete μ'_s values for each type of tissue, which were fitted with a curve described by the relation above.

d) After calculating $\mu_s(\lambda)$ and $\mu'_s(\lambda)$, $g(\lambda)$ could be calculated through the following relation [16]:

$$g(\lambda) = 1 - \frac{\mu'_s(\lambda)}{\mu_s(\lambda)} \tag{4}$$

e) The spectral dispersion ($n(\lambda)$) was calculated using the $\mu_a(\lambda)$ in the Kramers-Kronig (K-K) relations [17,18], first by introducing it in the following relation to obtain the imaginary part of the tissue dispersion ($\kappa(\lambda)$):

$$\kappa(\lambda) = \frac{\lambda}{4\pi}\mu_a(\lambda) \tag{5}$$

and then, using $\kappa(\lambda)$ in the following K-K relation [18] to obtain the real part of tissue dispersion:

$$n(\lambda) = 1 + \frac{2}{\pi}\int_0^\infty \frac{\lambda}{\Lambda} \times \frac{\lambda}{\Lambda^2 - \lambda^2}\kappa(\Lambda)d\Lambda \tag{6}$$

with Λ representing the integration variable over a wavelength range under consideration and λ representing a fixed wavelength within the range of interest that can be tuned for better adjustment of the calculated dispersion. To optimize this adjustment, a reference Cornu-type curve that was obtained from discrete RI measurements for each type of tissue was used [19]. The discrete RI values used to calculate the reference Cornu-type curves were experimentally obtained, both from healthy and from CRCC kidney samples, using the total internal reflection method [9]. Various lasers, emitting at different wavelengths between 400 and 860 nm, were used to perform these measurements from the kidney samples [19]. Individual measurements were made from three healthy and from three CRCC samples with each laser, allowing to obtain statistical data at each wavelength. Considering as an example the healthy kidney, once the mean RI values for all laser wavelengths were obtained, they were tested to see which of the dispersion curves described by the Cauchy, the Conrady and the Cornu equations provides a better fitting [9]. It was verified both for the healthy and for the CRCC kidney that the Cornu-type curve provides the best fitting of the experimental data [19].

f) Using the $\mu_a(\lambda)$ and the $\mu'_s(\lambda)$ it was possible to calculate the light penetration depth, $\delta(\lambda)$. According to literature [20], in a spectral range where $\mu_a \ll \mu'_s$, $\delta(\lambda)$ is calculated with the following relation,

$$\delta(\lambda) = \frac{1}{\sqrt{3\mu_a(\lambda)(\mu_a(\lambda) + \mu'_s(\lambda))}} \tag{7}$$

but for spectral ranges with strong absorption, when μ_a is comparable to μ'_s ($10\ \mu_a \geq 3\ \mu'_s$), $\delta(\lambda)$ should be calculated as follows [20]:

$$\delta(\lambda) = \frac{1}{\sqrt{\mu_a(\lambda)(\mu_a(\lambda) + 3\mu'_s(\lambda))}} \tag{8}$$

Considering the μ_a and μ'_s spectra obtained in the present study for the kidney tissues, the previous relation was used to calculate $\delta(\lambda)$ between 200 and 520 nm, while for higher wavelengths, the relation described by (7) was used for such calculation.

The averaged results of these calculations are presented in section 4 for both tissues.

4. Results and discussion

Fig. 2 shows the calculated $\mu_a(\lambda)$ and $n(\lambda)$ for the healthy and for the CRCC kidney.

Comparing between the calculated data in Fig. 2 for the healthy and for the CRCC kidney, it is seen that the two μ_a spectra are very similar, but the one for the CRCC kidney presents higher magnitude absorption bands, for DNA (260 nm), for hemoglobin at 415 nm (Soret) and at 540 and 570 nm (Q-bands) and for water at 975 nm [21]. The results presented in Fig. 2(C) and 2(D) show good agreement between the dispersions calculated with the K-K relations and the Cornu-type curves that result from discrete refractive index (RI) measurements made with similar tissues [19]. The CRCC kidney presents higher dispersion than the healthy kidney in the entire spectral range. Considering the Soret band at 415 nm in the dispersions obtained by the K-K relations, if we calculate the absorption fold-ratio between the peak of that band and the corresponding RI value in the Cornu-type curve, we see different values for the healthy and the CRCC kidney. In the case of the healthy kidney,

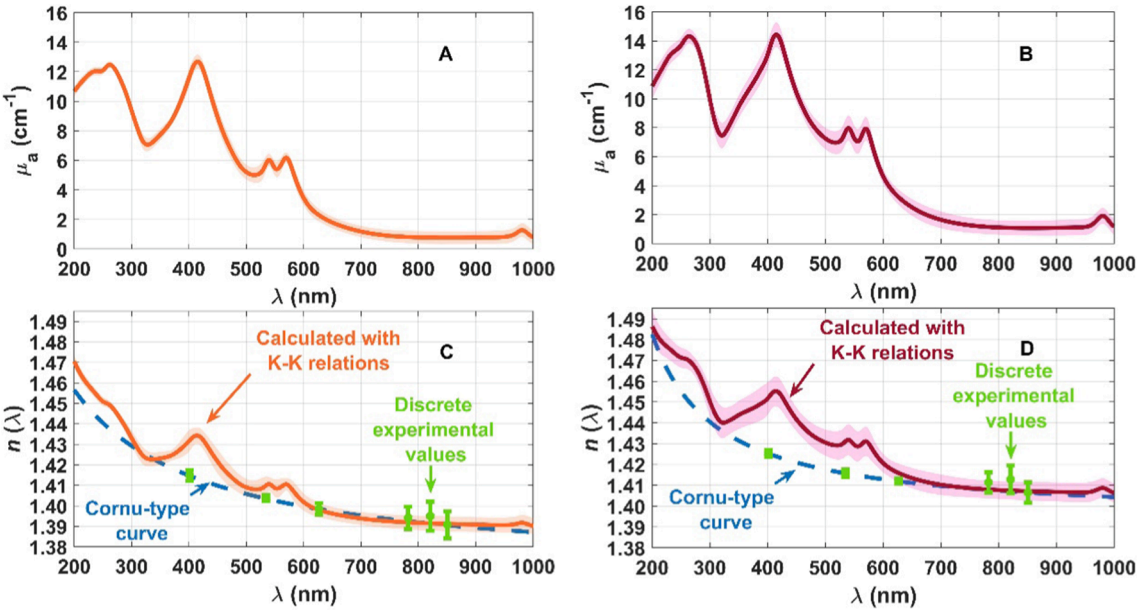

Fig. 2. Spectral μ_a of the healthy (A) and CRCC (B) kidney and spectral dispersion of the healthy (C) and CRCC (D) kidney.

such fold-ratio is 1.029 ± 0.006, while for the CRCC kidney it is 1.043 ± 0.010, showing that the diseased kidney presents a higher blood hemoglobin content. A similar calculation was made for the Q-bands, with the resulting mean fold-ratios also indicating a higher blood hemoglobin content in the CRCC kidney. Considering the healthy kidney, the fold ratios at 540 and 570 nm were 1.011 ± 0.005 and 1.013 ± 0.004, respectively, while for the CRCC kidney both ratios at those wavelengths were 1.023 ± 0.010. Although these calculated ratios suggest a higher blood hemoglobin content in the CRCC kidney, the distributions of values obtained for the two tissues are overlaid. A similar estimation of the absorption fold-ratios, which results in higher differences between the healthy and CRCC kidney, will be made later in this section, after we analyze and retrieve the pigments contributions from the absorption spectra of the kidney tissues.

Following the calculation procedure described in section 3, the spectra for μ_s and μ'_s were obtained for both tissues, as represented in Fig. 3.

The calculated μ'_s spectra that are presented in Fig. 3 show differentiating characteristics between the healthy and the CRCC kidney tissues. The estimated curves for these spectra, as described by relation (3), show that $f_{Ray} = 0.3125 \pm 0.0842$ and $b_{Mie} = 0.7822 \pm 0.3901$ for the healthy kidney, and that $f_{Ray} = 0.3417 \pm 0.0057$ and $b_{Mie} = 0.9880 \pm 0.0967$ for the CRCC kidney. Comparing between these results, we see that both f_{Ray} and b_{Mie} present similar values, or at least their value distributions regarding the healthy and the CRCC kidney are overlaid. This means that similar Rayleigh and Mie scattering regimes occur in both tissues. If, on the other hand, we consider only the mean estimated b_{Mie} values for the two tissues, the increase observed from the healthy to the CRCC kidney suggests that the average size of the Mie scatterers in the pathological tissue is higher than in the healthy kidney. These changes are certainly related to the development of higher sized and denser structures with a higher RI that occur during cancer progression, and further studies should be made to evaluate these parameters as cancer advances between stages. The establishment of a relation between f_{Ray} (or b_{Mie}) and the cancer stage of development could be useful for diagnostic/monitoring procedures. Fig. 3 shows that although both μ_s and μ'_s present a decreasing dependence on the wavelength, the magnitude values for these coefficients differ between the healthy and the CRCC kidney. An interesting feature that is observed in both tissues is that μ_s and μ'_s tend to match each-other near 200 nm, suggesting that scattering of light in the deep-UV tends to show zero anisotropy, as represented in Fig. 4.

As a result of calculations with the relation (4), indeed a nearly zero anisotropy was obtained for both tissues, as predicted in literature [15], and as already observed for other tissues [8–10]. The healthy kidney shows a faster increase in g than the CRCC kidney and an almost constant

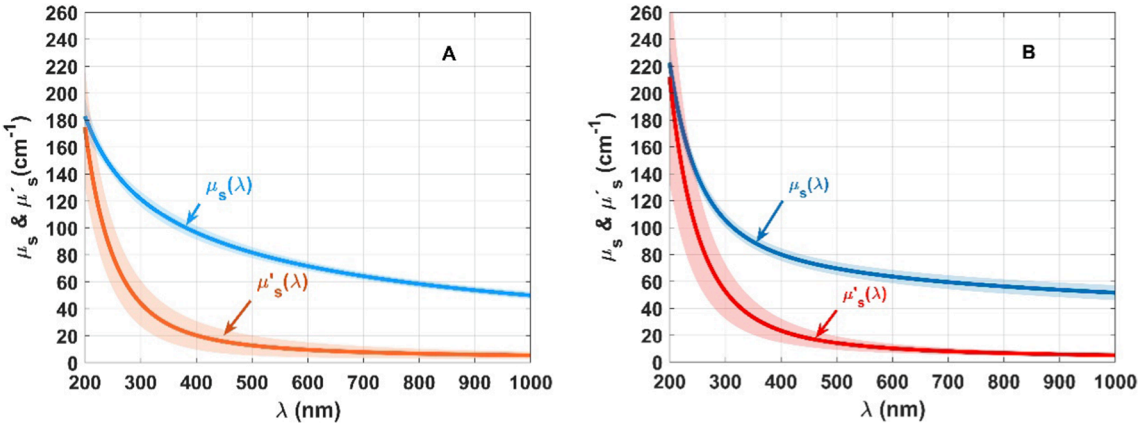

Fig. 3. Spectral μ_s and μ'_s of the healthy (A) and CRCC (B) kidney.

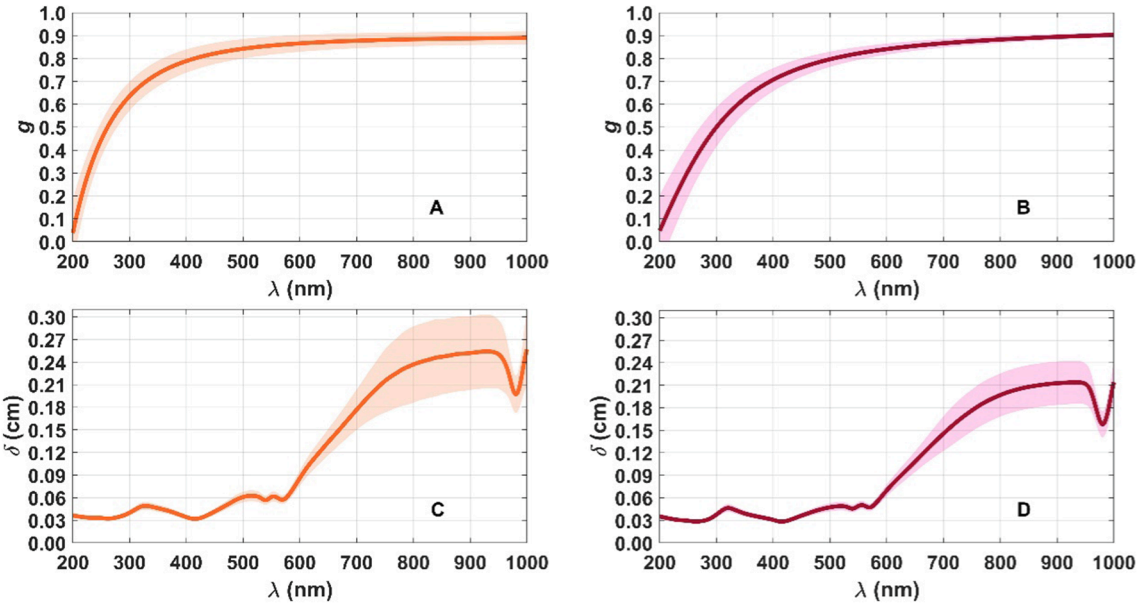

Fig. 4. Spectral *g* of the healthy (A) and of the CRCC (B) kidney, and spectral δ of the healthy (C) and CRCC (D) kidney.

anisotropy for wavelengths above 700 nm (Fig. 4(A)), while the CRCC kidney presents an almost linear increasing anisotropy for wavelengths above 600 nm (Fig. 4(B)).

Comparing between the spectra of δ that were calculated for both tissues, they present similar wavelength dependencies, but the values observed for the healthy kidney (Fig. 4(C)) tend to be higher than the ones observed for the CRCC kidney (Fig. 4(D)) for wavelengths above 400 nm.

After obtaining all the spectral optical properties of the kidney tissues, a further analysis on the μ_a spectra presented in Fig. 2(A) and in Fig. 2(B) was performed. Looking at those spectra, it is evident that both present a decreasing baseline from the deep-UV to the near infrared. In previous studies [8–10], the existence of such type of baseline was indicative of the presence of pigments in the tissues, namely melanin

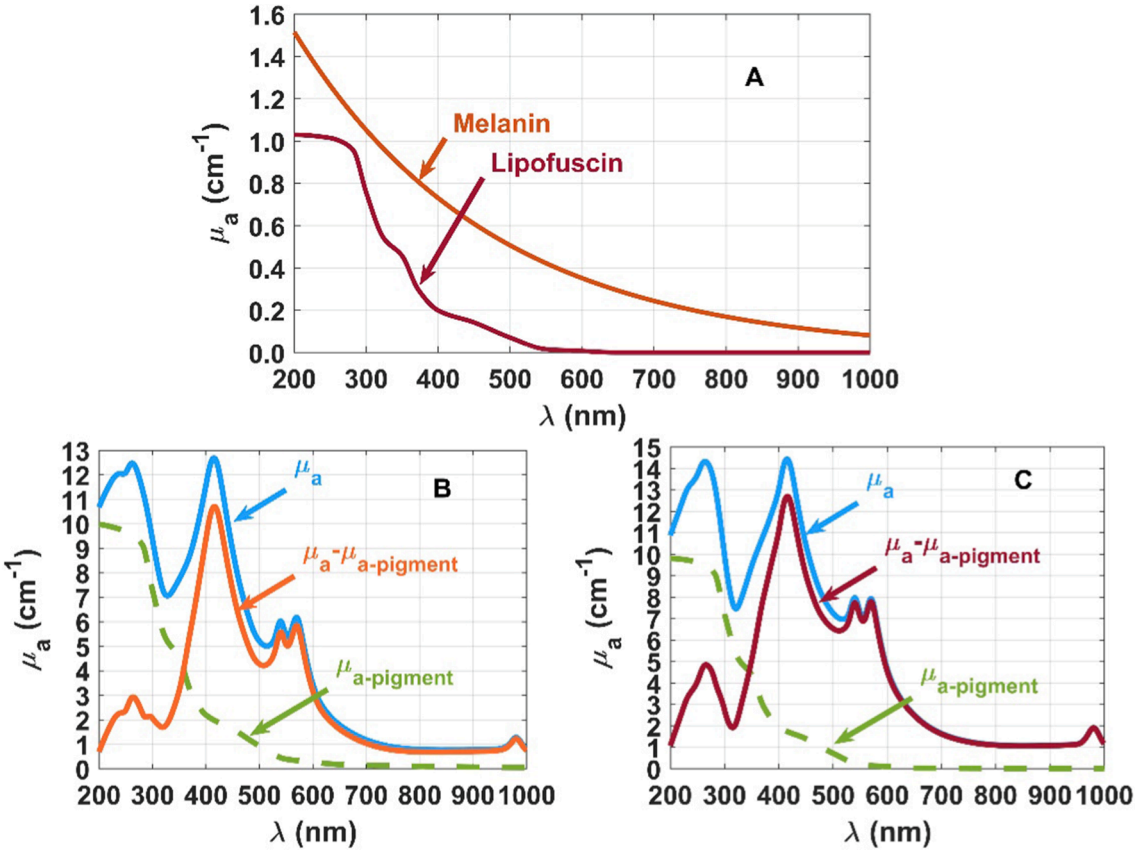

Fig. 5. Absorption spectra of melanin and lipofuscin (A), $\mu_a(\lambda)$ of the healthy kidney before and after subtracting the pigments contribution (B) and $\mu_a(\lambda)$ of the CRCC kidney before and after subtracting the pigments contribution (C).

and lipofuscin. According to literature [22], biological tissues accumulate both melanin and lipofuscin during the aging process, and these pigments contribute to cell degeneration.

The absorption spectra of melanin and lipofuscin are necessary to reconstruct that baseline for both kidney tissues. *Różanowska et al.* [23] have recently reported the absorption spectrum of lipofuscin between 200 and 1000 nm, and *Zonios et al.* [24] have previously reported the absorption spectrum of melanin in the same range. By retrieving data from Refs. [23] and [24], it was possible to reconstruct the absorption spectra of melanin and lipofuscin, which are represented in Fig. 5(A). Using these spectra, we combined them to reconstruct the baselines seen in the μ_a spectra of the healthy and of the CRCC kidney tissues presented in Fig. 2(A) and 2(B). When performing such combination for each tissue, numerical values were multiplied by the absorption spectra of melanin and lipofuscin, before adding the contributions of these two pigments to create the baseline. Those numerical values were optimized by trial-and-error for each tissue, so that the reconstructed baselines could match the ones seen in the μ_a spectra of both tissues that are presented in Fig. 2(A) and 2(B). By subtracting the reconstructed baselines to the mean curves presented in Fig. 2(A) and 2(B), the new absorption coefficient spectra of the kidney tissues were obtained with a horizontal baseline, as presented in Fig. 5(B) and 5(C).

Although the baselines ($\mu_{a\text{-pigment}}$) presented in Figures 5(B) and 5(C) seem equal, they are not exactly the same. They were reconstructed independently for each tissue with particular combinations of the spectra presented in Figure 5(A). For the case of the healthy tissue, such combination is described by the following relation:

$$\mu_{a-pigment}(\lambda) = 0.60 \times \mu_{a-mel} + 8.81 \times \mu_{a-lip} \quad (9)$$

where $\mu_{a\text{-mel}}$ and $\mu_{a\text{-lip}}$ represent the absorption spectra of melanin and lipofuscin, respectively, that are represented in Figure 5(A).

In the case of the CRCC kidney, the absorption pigment combination is described by:

$$\mu_{a-pigment}(\lambda) = 0.10 \times \mu_{a-mel} + 9.37 \times \mu_{a-lip} \quad (10)$$

Considering the numerical values used in the two previous relations as a measure of the melanin and lipofuscin contents in the kidney tissues, we see that a decrease in the melanin content (↓0.50) and an increase in the lipofuscin content (↑0.56) are observed from the healthy to the CRCC tissues. Such variations seem to suggest a conversion of about 83 % of melanin into lipofuscin from the healthy to the CRCC kidney. In a previous study [25], it was reported that melanin was produced from melanized lipofuscin in the presence of ferrous sulfide in brain tissues. Considering such production of melanin from lipofuscin, which is associated with the neurodegenerative process [25], and the conversion of melanin into lipofuscin suggested by the results in the present study, it seems that the interconversion of these pigments plays an important role in the development of certain health conditions. An alternative situation may have occurred in the kidney tissues studied in the present work. Instead of a conversion of melanin into lipofuscin, which has not been previously reported, the formation of melanolipofuscin granules may have occurred. Such formation of melanolipofuscin granules was previously reported for eye tissues and associated to the development of disease [26], and it consists on the aggregation of a lipofuscin shell around melanin. With the formation of such granules, the interaction of light is made only on the outside lipofuscin shell, which camouflages the melanin inside. Such fact may be a justification for the results obtained in the present study, but confirmation needs to be made in future studies. Considering still the data presented in Figure 5, some additional differentiating information between the healthy and CRCC kidney may be retrieved from the evaluation of the blood hemoglobin content. After subtracting the baselines from the μ_a spectra of both tissues, it is possible to quantify the blood hemoglobin contents in the healthy and in the CRCC kidney. Considering the Soret band at 415 nm, as previously done for the calculated dispersions in Fig. 2, if we consider the absorption fold-ratios to quantify the blood hemoglobin content in the tissues, different values are obtained for the healthy and for the CRCC kidney. In the case of the healthy kidney such fold-ratio is 15.72, while for the CRCC kidney it is 18.08. Once again, performing a similar calculation for the Q-bands, the fold-ratios at 540 and at 570 nm for the healthy tissue are 8.20 and 8.59, respectively, while for the CRCC kidney they are 10.80 and 10.81, respectively. Analyzing these data and the data obtained from the dispersions in Fig. 2, it seems that the calculation of the absorption fold-ratios at 415 nm, directly from the μ_a spectra after subtraction of the pigments absorption, is the one that presents more discrepancy between the healthy and the CRCC kidney. Either way, in all cases where these ratios were calculated it was observed a higher value for the diseased kidney, which shows that higher blood hemoglobin contents are found with the development of cancer. Consequently, the evaluation of the blood hemoglobin, melanin and lipofuscin contents and the interconversion of these pigments, or the formation of melanolipofuscin granules in biological tissues may provide information related to the progress of pathologies.

To summarize the differentiating data that was collected in the present study, Table 1 presents the estimated values for f_{Ray} and b_{Mie}, as estimated from the fitting of μ'_s data, along with the pigments contents and the absorption fold-ratios obtained at 415 nm after retrieving the absorption contributions of pigments from the μ_a spectra.

5. Conclusion

In the present study, a fast method was able to obtain all the spectral optical properties of human healthy and pathological kidney through direct calculation from *ex vivo* spectral measurements. Differences were detected when comparing between the spectral optical properties of the healthy and pathological kidney, but the absorption coefficient was the one that allowed to obtain a higher degree of differentiation. A higher blood hemoglobin content was found both in the absorption coefficient spectrum and in the tissue dispersion of the pathological kidney than the one observed for the healthy kidney. A reconstruction of the decreasing baseline observed in the absorption coefficient spectra of the kidney tissues suggests that 83 % of the melanin in the healthy tissue converts into lipofuscin in the pathological tissue. Such variations can be used as an optical marker of renal cancer. Future studies should concentrate on evaluating the melanin and lipofuscin contents, or confirmation on the formation of melanolipofuscin granules in kidney tissues at different stages of cancer development with the objective of developing new methods for diagnosis and for cancer stage detection.

CRediT authorship contribution statement

Ana R. Botelho: Investigation, Writing – review & editing. **Hugo F. Silva:** Investigation, Writing – review & editing. **Inês S. Martins:** Investigation, Writing – review & editing. **Isa C. Carneiro:** Investigation, Writing – review & editing. **Sónia D. Carvalho:** Investigation, Writing – review & editing. **Rui M. Henrique:** Supervision, Methodology, Writing – review & editing. **Valery V. Tuchin:** Conceptualization, Methodology, Writing – review & editing. **Luís M. Oliveira:** Conceptualization, Methodology, Writing – original draft.

Table 1
Differentiating data between healthy and CRCC kidney.

Parameter	Healthy kidney	CRCC kidney
f_{Ray}	0.3125 ± 0.0842	0.3417 ± 0.0057
b_{Mie}	0.7822 ± 0.3901	0.9880 ± 0.0967
Melanin content	0.60	0.10
Lipofuscin content	8.81	9.37
Mean absorption fold-ratio at 415 nm	15.72	18.08

Declaration of Competing Interest

The authors declare that they have no known competing financial interests or personal relationships that could have appeared to influence the work reported in this paper.

Data availability

Data will be made available on request.

Acknowledgements

The present work was supported by the Portuguese Science Foundation, grant n° FCT-UIDB/04730/2020.

Inês S. Martins was supported by the Portuguese grant FCT-UIDB/151528/2021.

The work of Valery V. Tuchin was supported by the Tomsk State University Development Programme (Priority-2030).

References

[1] R. Garje, D. Elhag, H. A. Yasin, L. Acharya, D. Vaena, L. Dahmoush, Comprehensive review of chromophobe renal cell carcinoma, Crit. Rev. in Oncol./Hematol. 160 (2021), 103287-1-6, 10.1016/j.critrevonc.2021.103287.

[2] G. Scelo, T. L. Larose, Epidemiology and risk factors for kidney cancer, J. Clin. Oncol. 36 (36) (2018), 3574-3581, https://ascopubs.org/doi/pdf/10.1200/JCO.2018.79.1905.

[3] W.M. Linehan, L.S. Schmidt, D.R. Crooks, D. Wei, R. Srinivasan, M. Lang, C. J. Ricketts, The metabolic basis of kidney cancer, Cancer Discov. 9 (8) (2019) 1006–1021, https://doi.org/10.1158/2159-8290.cd-18-1354.

[4] L. Fernandes, S. Carvalho, I. Carneiro, R. Henrique, V.V. Tuchin, H.P. Oliveira, L. M. Oliveira, Diffuse reflectance and machine learning techniques to differentiate colorectal cancer ex vivo, Chaos 31 (5) (2021), 053118, https://doi.org/10.1063/5.0052088.

[5] L. Oliveira, T. Gonçalves, M. Pinheiro, L. Fernandes, I. Martins, H. Silva, H. Oliveira, V. Tuchin, L. Oliveira, Invasive and minimally invasive optical detection of pigment accumulation in brain cortex, J. Biomed. Phot. & Eng. 8 (1) (2022), 010304.

[6] L. Wang, S.L. Jacques, L.Q. Zheng, MCML-Monte Carlo modeling of light transport in multi-layered tissues, Comp. Methods and Progr. In Biomedicine 47 (2) (1995) 131–146, https://doi.org/10.1016/0169-2607(95)01640-F.

[7] S.A. Prahl, M.J.C. van Gemert, A.J. Welch, Determining the optical properties of turbid media by using the adding-doubling method, Appl. Opt. 32 (4) (1993) 559–568, https://doi.org/10.1364/AO.32.000559.

[8] S. Carvalho, I. Carneiro, R. Henrique, V. Tuchin, L. Oliveira, Lipofuscin-type pigment as a marker of colorectal cancer, Electronics 9 (11) (2020) 1805, https://doi.org/10.3390/electronics9111805.

[9] T.M. Gonçalves, I.S. Martins, H.F. Silva, V.V. Tuchin, L.M. Oliveira, Spectral optical properties of rabbit brain cortex between 200 and 1000 nm, Photochem 1 (2) (2021) 190–208, https://doi.org/10.3390/photochem1020011.

[10] I.S. Martins, H.F. Silva, V.V. Tuchin, L.M. Oliveira, Fast estimation of the spectral optical properties of rabbit pancreas and pigment content analysis, Photonics 9 (2) (2022) 122, https://doi.org/10.3390/photonics9020122.

[11] B. Chance, M. Cope, E. Gratton, N. Ramanujam, B. Tromberg, Phase measurement of light absorption and scatterer in human tissue, Rev. Sci. Instrum. 69 (10) (1998) 3457–3481, https://doi.org/10.1063/1.1149123.

[12] A. V. Priezzhev, V. V. Tuchin, L. P. Shubochkin, *Laser Diagnostics in Biology and Medicine* (Nauka, Moscow, 1989).

[13] V. V. Tuchin, *Optical Clearing of Tissues and Blood* (SPIE Press, Bellingham, 2006).

[14] I. Carneiro, S. Carvalho, R. Henrique, L. Oliveira, V.V. Tuchin, Kinetics of optical properties of colorectal muscle during optical clearing, IEEE J. Sel. Top. Quant. Electr. 25 (1) (2018) 7200608, https://doi.org/10.1109/JSTQE.2018.2840346.

[15] S.L. Jacques, Optical properties of biological tissues: a review, Phys. Med. Biol. 58 (11) (2013) R37–R61, https://doi.org/10.1088/0031-9155/58/11/R37.

[16] A.N. Bashkatov, E.A. Genina, M.D. Kozintseva, V.I. Kochubei, S.Y. Gorodkov, V. V. Tuchin, Optical properties of peritoneal biological tissues in the spectral range of 350–2500 nm, Opt. Spectrosc. 120 (2016) 1–8, https://doi.org/10.1134/S0030400X16010045.

[17] J. Gienger, H. Gross, J. Newkammer, M. Bär, Determining the refractive index of human hemoglobin solutions by Kramers-Kronig relations with an improved absorption model, Appl. Opt. 55 (31) (2016) 8951–8961, https://doi.org/10.1364/AO.55.008951.

[18] O. Sydoruk, O. Zhernovaya, V. Tuchin, A. Douplik, Refractive index of solutions of human hemoglobin from the near-infrared to the ultraviolet range: Kramers-Kronig analysis, J. Biomed. Opt 17 (11) (2012) 115002.

[19] A. R. Botelho, *Determinação das propriedades óticas de tecidos e caracterização de tratamentos de transparência em rim humano normal e patológico*, MSc thesis, Polytechnic of Porto – School of Engineering (Portugal), November 2021, https://recipp.ipp.pt/handle/10400.22/19235.

[20] N. Honda, K. Ishii, Y. Kajimoto, T. Kuroiwa, K. Awazu, Determination of optical properties of human brain tumor tissues from 350 to 1000 nm to investigate the cause of false negatives in fluorescence-guided resection with 5-aminolevulinic acid, J. Biomed. Opt. 23 (7) (2018), 075006, https://doi.org/10.1117/1.jbo.23.7.075006.

[21] Y. Zhou, J. Yao, L.V. Wang, Tutorial on photoacoustic tomography, J. Biomed. Opt. 21 (6) (2016), 061007, https://doi.org/10.1117/1.JBO.21.6.061007.

[22] M.E. Gosnell, A.G. Anwer, J.C. Cassano, C.M. Sue, E.M. Goldys, Functional hyperspectral imaging captures subtle details of cell metabolism in olfactory neurosphere cells, disease-specific models of neurodegenerative disorders, Biochim. Biophys. Acta 1863 (1) (2016) 56–63, https://doi.org/10.1016/j.bbamcr.2015.09.030.

[23] M.B. Różanowska, A. Pawlak, B. Różanowski, Products of docosahexaenoate oxidation as contributors to photosensitizing properties of retinal lipofuscin, Int. J. Mol. Sci. 22 (7) (2021) 3525, https://doi.org/10.3390/ijms22073525.

[24] G. Zonios, A. Dimou, I. Bassukas, D. Galaris, A. Tsolakidis, E. Kaxiras, Melanin absorption spectroscopy: new method for noninvasive skin investigation and melanoma detection, J. Biomed. Opt. 13 (1) (2008), 014017, https://doi.org/10.1117/1.2844710.

[25] A. Moreno-Garcia, A. Kun, M. Calero, O. Calero, The neuromelanin paradox and its dual role in oxidative stress and neurodegeneration, Antioxidants 10 (1) (2021) 124, https://doi.org/10.3390/antiox10010124.

[26] S. Warburton, W. E. Davis, K. Southwick, H. Xin, A. T. Wooley, G. F. Burton, and C. D. Thulin, Proteomic and phototoxic characterization of melanolipofuscin: correlation to disease and model for its origin, Mol. Vis. 13 (2007), 318-329, http://www.molvis.org/molvis/v13/a35/.